REGULATORY INFORMATION DISTRIBUTION SYSTEM (RIDS)

ACCESSION NBR:7903210326 DOC.DATE: 79/02/14 NOTARIZED: NO DOCKET #
FACIL:50-305 KEWAUNEE NUCLEAR POWER PLANT, WISCONSIN PUBLIC SERVIC 05000305
AUTH.NAME AUTHOR AFFILIATION
JAMES,E.W. YA~~NKEE ATOMIC ELECTRIC~~ CO. WPSC
RECIP.NAME RECIPIENT AFFILIATION
SCHWENDER,A. OPERATING REACTORS BRANCH 1

SUBJECT: FORWARDS RESPONSES TO 790109 REQUEST FOR ADDL INFO RE "QUALIFICATION OF REACTOR PHYSICS METHODS FOR APPLICATION TO KEWAUNEE," ALONG W/REVISED PAGES.FORWARDS "RELOAD SAFETY EVALUATION METHODS," BOTH PROPRIETARY & NON-PROPRIETARY. (see reports)

DISTRIBUTION CODE: A001S COPIES RECEIVED:LTR 1 ENCL 0 SIZE: 401300
TITLE: GENERAL DISTRIBUTION FOR AFTER ISSUANCE OF OPERATING LIC

NOTES: I+E - 3 cys of all matl
LAWRENCE (OELD) - 1 cy All matl.

	RECIPIENT ID CODE/NAME	COPIES LTTR	COPIES ENCL	RECIPIENT ID CODE/NAME	COPIES LTTR	COPIES ENCL
ACTION:	05 BC ORB#1	7				
INTERNAL:	01 REG FILE	1	1	02 NRC PDR	1	1
	12 I&E	2	2	14 TA/EDO	1	1
	15 CORE PERF BR	1	1	16 AD SYS/PROJ	1	1
	17 ENGR BR	1	1	18 REAC SFTY BR	1	1
	19 PLANT SYS BR	1	1	20 EEB	1	1
	21 EFLT TRT SYS	1	1	22 BRINKMAN	1	1
EXTERNAL:	03 LPDR	1	1	04 NSIC	1	1
	23 ACRS	16	16			

Encl #1
~~REG FILE~~
NRC PDR
LPDR
L OLSHAN (1)
CORE PERF BR
REAC SFTY BR
ACRS (1)

Encl #2
REG FILE
L OLSHAN
CORE PERF BR
REAC SFTY BR
ACRS (1)

Encl #3 + #5
REG FILE
NRC PDR
LPDR
L OLSHAN
CORE PERF BR
REAC SFTY BR
ACRS (12)

LTR
A001

Encl #4
REG FILE
L OLSHAN (3)
CORE PERF
REAC SFTY BR
ACRS

MAR 26 1979

MA 2

GD

TOTAL NUMBER OF COPIES REQUIRED: LTTR 38 ENCL 0

WISCONSIN PUBLIC SERVICE CORPORATION

P.O. Box 1200, Green Bay, Wisconsin 54305

February 14, 1979

Mr. A. Schwencer, Chief
Operating Reactors Branch #1
Division of Operating Reactors
U. S. Nuclear Regulatory Commission
Washington, D. C. 20555

Gentlemen:

Kewaunee Nuclear Power Plant
Docket No. 50-305
Operating License DPR-43
Request for Additional Information Concerning
(A) "Qualification of Reactor Physics Methods for Application to Kewaunee" and (B) "Reload Safety Evaluation Methods for Application to Kewaunee"

Enclosed you will find the following:

1) Five (5) copies of our responses to your January 9, 1979, request for additional information concerning reference A topical report.
2) Five (5) copies of revised pages to the reference A topical report proprietary version.
3) Twenty (20) copies of revised pages to the reference A topical report non-proprietary version.
4) Five (5) copies of the proprietary version of the reference B topical report.
5) Twenty (20) copies of the non-proprietary version of the reference B topical report.

The enclosed responses to your request for additional information along with the second topical report, reference B, complete the responses to your first-round questions.

Very truly yours,

E. W. James, Senior Vice President
Power Supply and Engineering

snf

Enc.

7903210326

A001 (LTR) 1/0 ENCL TO LIST

REGULATORY DOCKET FILE COPY

18

UNITED STATES
NUCLEAR REGULATORY COMMISSION
WASHINGTON, D. C. 20555

MEMORANDUM FOR: TERA Corp.

FROM: US NRC/TIDC/Distribution Services Branch

SUBJECT: Special Document Handling Requirements

☑ 1. Please use the following special distribution list for the attached document.

ENCL #1
REG FILE
NRC PDR
LPDR
L OLSHAN (1)
CORE PERF BR
REAC SFTY BR
ACRS (1)

ENCL #2
REG FILE
L. OLSHAN
CORE PERF BR
REAC SFTY BR
ACRS (1)

ENCL #3 & #5
REG FILE
NRC PDR
LPDR
L OLSHAN
CORE PERF BR
REAC SFTY BR
ACRS (12)

LTR
A001

ENCL #4
REG FILE
L OLSHAN (3)
CORE PERF
REAC SFTY BR
ACRS

~~LTR A001~~

☑ 2. The attached document requires the following special considerations:

☐ Do not send oversize enclosure to the NRC PDR.

☐ Only one oversize enclosure was received - please return for Regulatory File storage.

☑ Proprietary information - send ~~affidavit~~ LTR UNP only to the NRC PDR

☑ Other: (specify)

NO TERA CY OF ENCL'S

Mike Collins

cc: DSB Files

TIDC/DSB Authorized Signature

DOCKET NO. 50-305

DATE: 3-26-79

NOTE TO NRC AND/OR LOCAL PUBLIC DOCUMENT ROOMS

The following item submitted with letter dated 2-19-79 from Yankee Atomic Elec. Co. is being withheld from public disclosure in accordance with Section 2.790.

PROPRIETARY INFORMATION

Request for Addl. Info re qualification of reactor Physics methods for application to [redacted] Kewaunee along revised pages

Roland Wood
O/b

Distribution Service's Branch

ENCLOSURE 1

RESPONSES TO REQUESTS FOR ADDITIONAL INFORMATION

10. Kewaunee measurements for Cycles 1, 2, and 3 have been used to benchmark the WPSC ARMP model and quantify the reliability factors. However, most of the data is from Cycle 1. The Doppler reactivity effect includes only Cycle 1 results and the isothermal temperature coefficient includes only one measurement from Cycle 2 and none from Cycle 3. Justify the adequacy of the reliability factors derived in this report for other than Cycle 1 predictions.

RESPONSE: Conservative acceptance criteria utilizing only those measurements with both heatup and cooldown data for ITC qualification, precluded the use of all but the six measurements employed in the original qualification of the reliability factors. The acceptance criteria has been re-evaluated since it has been found that heatup and cooldown ITC measurements yield consistent results when adequate RCS stabilization is achieved. New acceptance criteria requiring large reactor coolant system stabilization time was adopted. Thus measurements from Cycle 3 and 4 have been added to the data base and the reliability factors requantified. The revised values are presented in Table 3.5. Comparisons for reload cycles 2, 3, and 4 show measurement differences well within the calculated reliability factor.

No measurements of power coefficient were made after Cycle 1 in the Kewaunee reactor. Therefore, the justification of the adequacy of the reliability factor for advanced cycles must be qualitative. In advanced cycles, the only component of the coefficient that is not present during the early part of Cycle 1 is PU-240, which can contribute up to 15% of the doppler effect depending on the fuel exposure. Section 3.4 of the report excerpts results from the ARMP documentation and demonstrates the capability of the analytical model to adequately determine the concentration of PU-240. Therefore, it is expected that the analytical

model will predict power (or doppler) coefficients satisfactorily in future cycles.

11. Describe in more detail the determination of the albedoes used in the nodal code to calculate power distributions. Are they power dependent? Are they adjusted as a function of burnup? How are they determined for pre-operational predictions?

RESPONSE: The radial determination of the nodal model albedoes is performed by comparison of power distributions to the quarter core PDQ model under full power, unrodded, BOC conditions. The resultant radial albedoes are neither burnup nor power dependent for a given cycle, as is evidenced by the good agreement of measured versus calculated power distributions from BOC to EOC. The radial normalization used for the Cycle 1, 2 and 3 benchmark calculations were performed in this manner and the resulting power distributions presented in Section 3.5 of the report.

The axial albedoes were determined by comparison to Cycle 1 Incore flux measurements and have remained constant for Cycles 2, 3 and 4.

These same radial determination techniques and the constant axial values are employed for preoperational predictions.

12. There is confusion in the statistical argument starting on page A-4 among the "true" values, the "observed" values, and the "fixed" values. In any event, this derivation is unnecessary since tables of one and two-sided tolerance limits exist. In addition, Appendix A.2 does not yield a good approximation to the tolerance factors. For example, the isothermal temperature coefficient reliability is computed on page 3-10 as 2.44 σ. Explain this apparent non-conservatism in your statistical method.

RESPONSE: The argument beginning on page A-4 is not intended for the estimation of tolerance factors. Its purpose is to augment the conservatism of the tolerance factors employed.

The approximation of the tolerance factors used in Appendix A-2 was based on large sampling theory for sample sizes of $N > 30$. This yielded an erroneous approximation to the tolerance factors, since small sampling theory was appropriate due to the small number of samples employed. The ITC reliability factor has been re-calculated using small sampling theory. Revision pages for 3-10, 3-11, and A-7 are attached to implement this correction as well as to employ the additional data points added in response to question No. 10

13. The statistical analyses used to determine the uncertainties applicable to nodal power distributions (Section 3.5) assume normal distributions and pooling. Have any statistical tests such as the W-test or the Bartlett test been performed to validate these assumptions? If not, we request that you perform these tests and report the results

RESPONSE: Previous statistical analyses used to determine the uncertainties applicable to nodal power distributions assume normal distributions and pooling. Pooling is valid only if the apparent differences in cycle specific statistics are not significant at the 95% confidence level. However, the Bartlett test has been performed and has shown that these apparent differences are significant at the 95% confidence level and thus pooling is not valid. Therefore, a conservative upper bound to the cycle specific σ_{NODE} values is to be used instead of the σ_{NODE} values derived from the cycle pooling statistics.

The nodal power distribution uncertainties, σ_{NODE}, for each cycle are computed using the standard deviation of the differences between the measured and predicted instrument signals and the measurement uncertainties. The individual cycle uncertainties are shown in the attached Figure 1 as a function of core axial level. In order to ensure conservatism in the values of σ_{NODE}, a conservative upper bound to the individual cycle results must be employed. This upper bound is represented by the solid line in Figure 1.

Note that the Cycle 4 data, which was not used in the determination of the D1 and D2 factors, is below the upper bound to σ_{NODE} in Figure 1.

In a similar fashion, an upper bound value has also been chosen for σ_{ASSY}.

FIGURE 1

CYCLE SPECIFIC VALUES OF SIGMA NODE
FOR KEWAUNEE

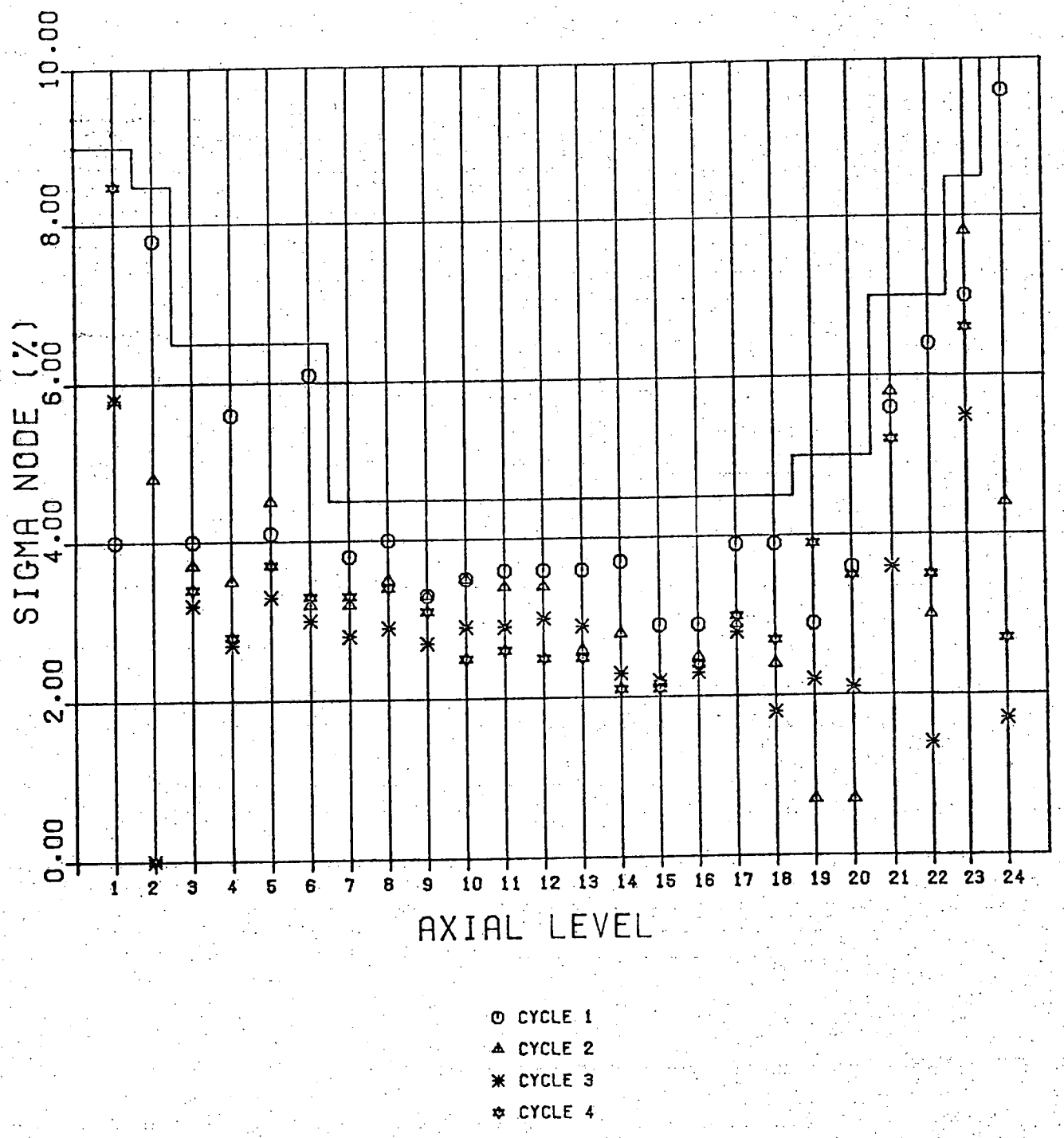

14. Explain the value of 1.3 $\pm$ 0.4% quoted as the 95% confidence limits of σ(CPM) for a sample size of 15 (page 3-101). The one-sided 95/95 tolerance interval for CPM is bias + Kσ(CPM), or -0.7 + (2.566)(1.3) = 2.64.

RESPONSE: Although the one-sided 95/95% tolerance interval for CPM is defined as -0.7 + (2.6)(1.3), what is of concern on page 3-101 is the upper one-sided 95% confidence limit to the standard deviation of the sampling distribution for σ(CPM).

According to small sampling theory, this interval is estimated as:

$$\sigma^2 < \frac{N-1}{\chi^2_\alpha} S^2 = \frac{14}{6.57} S^2 = 1.46^2 S^2$$

$$\sigma < (1.46)(1.3) = 1.90 = 1.3 + 0.6\%$$

Based on this, the estimate of 1.3 + 0.4% presented in the report is slightly non-conservative and should be corrected with the above results.

A revision to page 3-101 is attached to implement this modification.

15. The method of combining uncertainties to determine the F_Q^N reliability factors appears inaccurate.

$$(RF)^2 = K\sigma_{FQ}^2 = K_{nodal}\ \sigma_{nodal}^2 + K_{PDQ}\ \sigma_{PDQ}^2 = K(\sigma_{NODAL}^2 + \sigma_{PDQ}^2)$$

only if $K_{nodal} \approx K_{PDQ}$. Since there is a fair amount of data, K_{nodal} may well be 1.65. However, for only 15 samples, K_{PDQ} should be much larger. Explain.

RESPONSE: There appears to be confusion in the method of combining uncertainties and the definition of the K factors. The following discussion is offered for clarification.

The method of combining uncertainties to determine the F_Q^N reliability factors was to choose a large upper bound on σ_{PDQ} such that it conservatively encompassed the K factor appropriate to σ_{PDQ}. However, the proper treatment for combining the uncertainties is as follows:

$$RF = (\overline{X}_{PDQ} + K_u S_{PDQ}) + \sqrt{1.645^2 (K_{\sigma NODAL}^2 * \sigma_{NODAL}^2 + K_{\sigma PDQ}^2 * \sigma_{PDQ}^2)}$$

where: 1. The K_σ-factors are those appropriate to the one-sided 95% confidence interval for σ.

2. The K_u-factor is the critical factor for the one-sided confidence interval for the mean.

In this treatment, employed in the attached revision pages, the calculated K-factors are explicitly used in combining the CPM and PDQ uncertainties, and the σ_{PDQ} used is the best fit rather than a conservative upper bound. The result, as presented in the revised page 3-103 is:

$$\sigma^2(PDQ\text{-}MEAS) = K_{\sigma PDQ}^2 \sigma_{PDQ}^2 \leq 2.0\%$$

Since $K_{\sigma NODAL}$ is approximately 1.0 due to the large number of data points, the reliability factor for F_Q^N becomes:

$$RF = (\overline{X}_{PDQ} + K_u S_{PDQ}) + 1.645\sqrt{\sigma^2_{NODAL} + \sigma^2_{(PDQ-MEAS)}}$$

The revised reliability factors are presented in the attached revision to page 3-118.

16. Our calculations show the minus sign in the derivation of Equation A-6 to be in error. Verify your result.

RESPONSE: The minus sign in equation A-6 is in error. However, this error has no impact on the application of A-6 since the procedure for such applications described on page A-5 forces ε to be positive or zero. A revision to page A-5 is attached to correct the error.

17. Regarding the figures referred to at the bottom of page A-5 (not tables), the value obtained from Fig. 3.8, nodes 3 and 4 has the wrong sign. Correct your result.

RESPONSE: The sign used in the example at the bottom of page A-5 was changed to assure $\varepsilon \geq 0$ in accordance with the procedure defined on page A-5.

The sign has been corrected consistent with the correction discussed in the response to question 16. Revisions to page A-5 and A-6 are attached to reflect this change.

Enclosure 2

Revisions to Topical Report titled, "Qualification of Reactor Physics Methods for Application to Kewaunee".

3.2 Temperature Coefficient Benchmarking

Measurements of the isothermal temperature coefficient at HZP are adequately made with a reactivity computer as there is usually no rod motion. When there is rod motion, there is usually sufficient time to allow the flux to stabilize.

The comparisons to the WPS ARMP model are summarized in Table 3.5 and Figure 3.2. It is apparent that a constant bias of -3.4 pcm/F exists with an RMS * scatter of 1.8 pcm/F.

---

*Root mean square = 1σ

The ITC reliability is defined as $\pm$ 5.7 pcm/F which represents a 95% probability ($\pm 1.65\sigma$) at the 95% confidence level that the measured ITC will be bounded by the predictions when the bias is included.

Revised 1/31/79

TABLE 3-5

MEASURED & CALCULATED ISOTHERMAL TEMPERATURE COEFFICIENTS

BOC, HZP, Kewaunee Cycles 1-4

Cycle	Rod Position Bank	Rod Position Steps	T_{MOD} (F)	Boron (ppm)	ITC $(\frac{pcm}{F})$ Meas.	ITC $(\frac{pcm}{F})$ Calc.	Diff pcm/F
1	D	190	538	1583	-2.4	- 4.9	-2.5
	C	196	540	1450	-3.6	-7.8	-4.2
	B	189	542	1317	-7.5	-12.4	-4.9
	A	201	545	1227	-11.3	-18.5	-7.2
	SB	194	544	1011	-14.1	-17.7	-3.0
2	D	204	540	1346	-4.0	-6.2	-2.2
3	D	162	540	1496	-4.4	-6.6	-2.2
4	D	200	543	1488	-3.9	-4.9	-1.0

Average difference = -3.4 $(\frac{pcm}{F})$

St'd deviation about avg. = 1.8 $(\frac{pcm}{F})$

FIGURE 3.2

MEASURED TO CALCULATED ISOTHERMAL TEMPERATURE COEFFICIENT DIFFERENCE VERSUS BORON

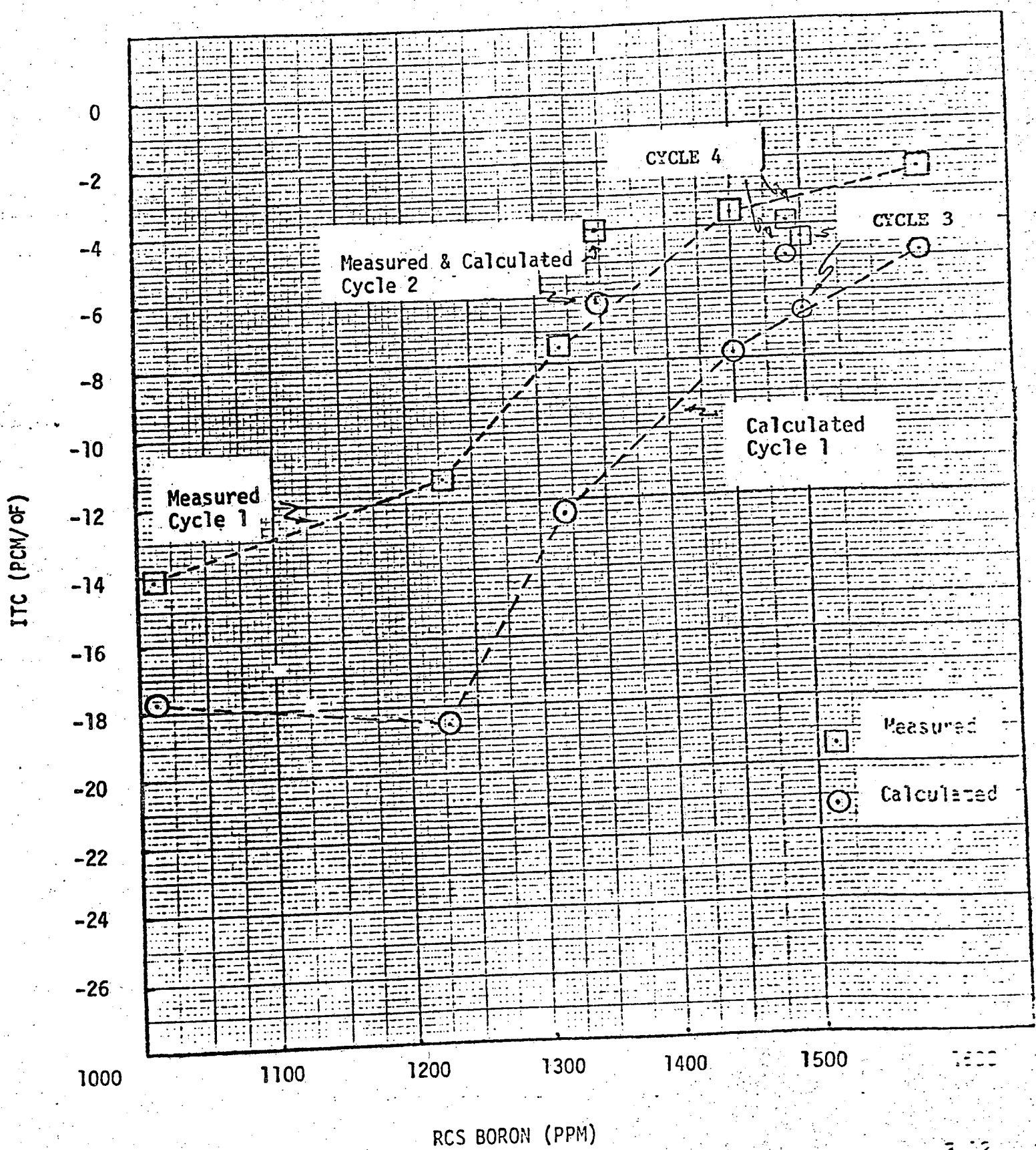

simulated with the WPS ARMP model. In addition to the measured signals from the moveable in-core fission detectors, core exit thermocouple data are also available from the ejected and dropped rod tests, and comparisons to model predictions of both in-core detectors and thermocouples are presented in Section 3.6.

The calculation of peaking factors for Kewaunee safety evaluations is performed in a multi-step process beginning with the nodal code. For any core condition, the three-dimensional power distribution is calculated with 12-node axial resolution. The nodal values are then split axially with a single set of constant factors which account for the average axial flux gradients within a node and local flux perturbations caused by the assembly grid straps. The derivation of these factors is explained below.

In order to derive uncertainty factors consistent with the above methodology, direct comparisons were made of the predicted and measured reaction rates in each half-node region for all flux maps tabulated in Table 3.8.

Each of the 19 flux maps consists of 61 measured axial data points in each of the 36 instrumented locations. These 61 values were grouped into approximately 3 points per ½-node. The total data base is therefore in excess of 40,000 measured data points.

The standard deviation (average deviation, M, fixed as zero. See Appendix A.2) of the differences between the predicted peak axial reaction rate and the actual peak axial reaction rate (one of the three points) in each half-node has been calculated for each of the three cycles.

These results represent the combined effects of model accuracy and measurement uncertainty. It remains to conservatively estimate the model accuracy component using the statistical methods described in Appendix A.

In Figure 3.6, differences between measured and calculated incore detector signals are plotted as histograms.

In Figure 3.6A, measured and calculated channel integrated in-core detector signals are compared for steady state reactor conditions over the first three cycles of Kewaunee operation. In Figures 3.6B and C, maximum point values in each instrumented ½-node are compared for the same reactor state points.

The nodal power distribution uncertainties for each cycle have been computed with the standard deviation of the differences between the measured and predicted instrument signals, the measurement uncertainties and equation A-5. The overall model uncertainty, σNODE, has been defined as a conservative upper bound to the individual cycle uncertainties.

The data shown in Figure 3.6A demonstrate that the combined effects of measurement uncertainty and calculational uncertainty yield a difference distribution with a standard deviation of 2.5% for channel integrated signals.

The assembly average power distribution uncertainties have been calculated using equation A-5. In a manner similar to that used for σNODE, the overall model uncertainty, σASSY, appropriate to the assembly average power distributions has been defined as a conservative upper bound to the individual cycle results.

$$\sigma ASSY = 0.027$$

A few of the individual comparisons of the measured and predicted reaction rates used to derive the uncertainties in Table 3.9 are shown in Figures 3.9 to 3.56. For each map, the differences in the channel and integrated values are shown along with the actual axial plots for an inner and outer instrument location. It should be noted that the axial plots have not been renormalized to make the integrals equal. The particular locations were chosen such that data would be available for each map. The inner thimble (#1) is the calibration thimble which is always measured and the outer thimble is either J3 (#24) or K4 (#31) which are nearly geometrically symmetric.

TABLE 3.8

MEASURED IN-CORE DETECTOR REACTION RATE DISTRIBUTIONS

KEWAUNEE

Fuel Cycle	Flux Map No	Cycle Exposure (GWD/MTU)	Power Level (%)	Rod Position (Steps)	Comments
1	1	0	~5	D=205	BOL, HZP
	12	0.2	37	D=152	K7 Ejected
	15	0.2	50	D=196	K7 Dropped
	34	1.8	92	D=198	
	66	6.6	97	D=218	
	108	12.6	98	D=217	
	131	16.2	98	D=217	EOC
2	133	0	~5	D=223	BOC, HZP
	154	1.4	100	D=219	
	163	3.5	96	D=223	
	179	6.1	97	D=225	
	194	8.5	98	D=228	EOC
3	195	0	~5	D=220	BOC, HZP
	207	1.4	98	D=228	
	215	3.4	99	D=228	
	221	5.9	100	D=228	
	235	10.0	100	D=228	
	244	12.8	99	D=228	EOC

TABLE 3.9

NODAL UNCERTAINTIES FOR KEWAUNEE

	NODE	½-NODE	σ_{NODE}	AXIAL FACTORS D1		D2
(core top)	12	24	.077	.857		1.171
		23	.067	1.238		1.053
	11	22	.034	.985	*	1.073
		21	.045	1.126		1.029
	10	20	.030	1.045		1.011
		19	.029	1.051		1.012
	9	18	.030	.949	*	1.050
		17	.036	1.028		1.010
	8	16	.030	1.021		1.005
		15	.029	1.021		1.004
	7	14	.031	.948	*	1.055
		13	.035	1.000		1.018
	6	12	.037	1.012		1.004
		11	.036	1.018		1.002
	5	10	.037	.983	*	1.021
		9	.037	.954	*	1.054
	4	8	.038	1.007		1.006
		7	.037	1.015		1.006
	3	6	.046	1.013		1.011
		5	.043	.936	*	1.051
	2	4	.049	1.041		1.016
		3	.042	.962		1.042
(core bottom)	1	2	.053	1.099		1.147
		1	.077	.666	*	1.166

*Approximate grid strap locations

The standard deviation about this bias is then 1.9%.

The CPM calculational uncertainty can now be computed using equation A.5 as shown below.

The one-sided, 95/95, confidence limit of σ(CPM) for a sample size of 15 is 1.3 + 0.6%.

A benchmark comparison of PDQ to CPM is described in Part I, Chapter 4 of the ARMP documentation. These results are reproduced in Figure 3.79 and tabulated in Table 3.13. The average (PDQ - CPM) peak pin bias for fuel pins adjacent to the water holes is +0.5% with a 1σ scatter about this bias of + 0.5%. These calculations represent a 14 x 14 fuel assembly at zero power and no burnup. In order to better define the PDQ - CPM differences for application to Kewaunee, new calculations were performed which compared the WPS ARMP models with CPM.

The WPS PDQ - CPM comparison calculations were made for a typical fuel type of 3.03 w/o over a burnup range of 0 to 18.0 GWD/MTU. The individual PDQ and CPM pin power distributions for the BOC and EOC cases are shown in Figures 3.80, 81 and 82. The differences between the PDQ and CPM pin powers for all fuel pins of higher than average power density are tabulated in Table 3.14. Since the average pin power has been normalized to unity, the values shown are typical of the peak pin to box ratios that might be applied to the peak nodal values of section 3.5 to compute the local F_Q^N values. (In actual practice, the values would be computed from quarter core rather than assembly geometry.)

The WPS calculations are consistent with the PDQ - CPM comparisons described in the ARMP documentation. Both demonstrate that PDQ overpredicts the peak pins relative to CPM. The WPS results demonstrate the fact that PDQ, with MND (mixed number densities), over-predicts the power in the fuel pins relative to CPM near the water holes. The lower bound of the peak pin to box (assembly average) power ratio as calculated by PDQ for Kewaunee is about 1.10. The average difference between

PDQ and CPM for peak pin to box ratios of 1.10 is 2.1%. This is obtained from a linear fit of the BOC and EOC pin-to-box differences in Table 3.14 versus the pin-to-box ratio. The standard deviation of the data about the line of best fit is 0.4%.

The uncertainties of CPM have now been defined with respect to experiment and the uncertainty of PDQ with respect to CPM. For conservatism, the uncertainty of PDQ with respect to experiment is defined as the statistical sum of the upper one-sided 95% confidence limits of σ(CPM-Meas) and σ(PDQ-CPM). These limits are as follows.

σ(CPM-Meas) < .019% (95% confidence, sample size N_1=15)

σ(PDQ-CPM) < .006% (95% confidence, sample size N_2=20)

$$\sigma(\text{PDQ-Meas}) < \sqrt{(.019)^2 + (.006)^2} = 2.0\%$$

The PDQ-Measurement bias is simply the sum of the CPM-Measurement bias and the PDQ-CPM bias (the bias is the negative of the average difference).

$$\begin{aligned}\text{Bias (PDQ-Meas)} &= \bar{x}(\text{CPM-Meas}) + \bar{x}(\text{PDQ-CPM}) \\ &= +0.7\% - 2.1\% \\ &= -1.4\%\end{aligned}$$

The lower, one-sided 95% confidence limit for difference between these two means is obtained from small sampling theory as -0.8% (sample sizes N_1=15, N_2=20)

Bias (PDQ-Meas) < -1.4% + 0.6% = -0.8%

However, for added conservatism, the PDQ bias will be defined as only half this magnitude, or only -0.4%.

In summary then, the statistics associated with PDQ calculations of peak pin-to-assembly average power ratios are as follows:

σ(PDQ-Meas) $\leq$ 2.0%

bias(PDQ-Meas) = -0.4%

TABLE 3.10

KRITZ EXPERIMENTS FOR

PWR LATTICES

PWR lattice 470F, <100 ppm

15x15 MO_2 assembly with water holes and absorber rods surrounded by a uniform UO_2 lattice (Fig 3.75)

Pu content in the MO_2 rods	1.5 %
UO_2 rod enrichment	1.9 %.

PWR lattice 470F, 1000 ppm

14x14 MO_2 assembly with graded enrichment and with water holes, surrounded by UO_2 assemblies (Fig 3.76)

Pu content in the MO_2 rods	2 and 3 %
UO_2 rod enrichment	3 %.

3.7.2 F_Q^N Reliability Factors

As explained in Section 3.5, the local pin peaks, F_Q^N, are calculated by multiplying peak nodal values by the PDQ pin-to-box ratios. These components are nearly independent in that the PDQ pin-to-box ratios are insensitive to changes in assembly power level, xenon inventory and boron concentration. Statistically as described below:

$$\sigma_{FQ}^2 = \sigma_{NODE}^2 + \sigma_{PDQ}^2$$

σ_{NODE} = Upper bound to the nodal uncertainties defined in Table 3.15

σ_{PDQ} = Upper, one-sided 95% confidence limit derived in section 3.7.1

σ_{FQ} = Upper, one-sided 95% confidence limit for the FQ uncertainty

The 95/95% confidence level reliability factors for F_Q are computed from the σ_{FQ} values above and the lower, one-sided 95% confidence limit for the PDQ bias defined in section 3.7.1. The results are shown by axial level in Table 3.15.

TABLE 3.15

F_Q^N RELIABILITY FACTORS FOR KEWAUNEE

	NODE	1/2 NODE	σNODE	F_Q RELIABILITY FACTORS (95/95% CONFIDENCE LEVEL)
(core top)	12	24	.100	.165
		23	.085	.140
	11	22	.070	.116
		21	.070	.116
	10	20	.050	.085
		19	.050	.085
	9	18	.045	.077
		17	.045	.077
	8	16	.045	.077
		15	.045	.077
	7	14	.045	.077
		13	.045	.077
	6	12	.045	.077
		11	.045	.077
	5	10	.045	.077
		9	.045	.077
	4	8	.045	.077
		7	.045	.077
	3	6	.065	.108
		5	.065	.108
	2	4	.065	.108
		3	.065	.108
(core bottom)	1	2	.085	.140
		1	.090	.148

3.7.3 $F_{\Delta H}$ Reliability Factor

The peak pin $F_{\Delta H}$'s are calculated as products of the nodal assembly average power values and the PDQ peak pin-to-box ratio.

In Section 3.5 the uncertainty (σ_{ASSY}) appropriate to the nodal assembly average power calculations was determined to be 2.7%. This is combined with the PDQ pin-to-box uncertainty (σ_{PDQ}) of 2.0% from section 3.7.1. to obtain σ_{FH}, the upper, one-sided 95% confidence limit for the $F_{\Delta H}$ in a manner similar to that of Section 3.7.2.

The 95/95% confidence level reliability factor appropriate to $F_{\Delta H}$ is then computed from the value of σ_{FH} above and the lower, one-sided 95% confidence limit for the PDQ bias defined in section 3.7.1.

$\sigma_{FH} = 0.051$

3.8 Delayed Neutron Parameters

The importance of the reliability of the calculated values of the delayed neutron parameters is primarily associated with the core β_{eff}. The uncertainties in the calculation of β_{eff} are composed of several components, the most important of which are listed below:

a. Experimental values of β, and λ, by nuclide;

b. Calculation of the spatial nuclide inventory. These uncertainties are addressed in Section 3.4;

c. Calculation of core average β as a flux weighted average over the spatial nuclide inventory;

d. Calculation of β_{eff} from the core average as $\beta_{eff} = \bar{I} * \beta$, where $\bar{I}$ = importance factor.

The experimental determinations of the β 's and λ 's are assumed to be accurate to within 1%. The most important nuclide concentrations with respect to core β are U^{238}, U^{235} and Pu^{239}. Table 3.7 of Section 3.4 demonstrate that the uncertainty in the calculation of these parameters is about 0.3% or less. Therefore, components a) and b) above are combined as 1.3%.

The uncertainty in the calculation of a core average β depends on the relative flux weighting of the individual assemblies in the core. For demonstration purposes, consider a three region core, each with a different average burnup and average β. This is typical of advanced PWR cycles in that about a third of the core has seen two previous cycles, a third only one previous cycle and a third is the feed fuel. Typical regional β's are given below:

A.1 Separation of Measurement and Calculational Uncertainties

Comparisons of measured and calculated reactor parameters include the effects of both the measurement and calculational uncertainties. Methods used in this report to isolate the calculational uncertainties are described below in terms of the following definitions:

X_T = true reactor parameter

X_M = measured reactor parameter

X_C = calculated reactor parameter

$e_M = X_M - X_T$ = measurement error

$e_C = X_C - X_T$ = calculation error

$e_{MC} = X_M - X_C$ = observed differences

$\mu_i = \bar{e}_i$ = mean error

$\sigma_i = \sqrt{\frac{1}{N}\Sigma(e_i - \mu_i)^2}$ = standard deviation

$m_i^2(A) = \frac{1}{N}\Sigma(e_i - A)^2$ = second moment about an arbitrary origin A

If e_M and e_C are independent, then the following relationships exist.[7,8]

(A - 1) $\sigma_C^2 = \sigma_{MC}^2 - \sigma_M^2$

(A - 2) $\mu_C = \mu_M - \mu_{MC}$

Once the σ_C and μ_C have been calculated from historical data, they could be used to apply conservatism to future calculations of reactor parameters, X_C, as follows:

(A - 3) $X_C' = X_C - \mu_C \pm r_1 r_2 \sigma_C$

The factors r_1 and r_2 are defined as described in Section A.2 to provide a 95% probability at the 95% confidence level that X_C' is conservative with respect to the true value, X_T.

A.2 Reliability Factors

It is the objective of this section to define reliability factors which are to be used to increase/decrease calculated results to the point where there is a 95% probability at the 95% confidence level that they are conservative with respect to actual reactor performance. Thus there are two components to be considered, termed r_1 and r_2.

A distribution of differences between truth and calculation for a given parameter is characterized by its standard deviation, σ_C. The first component, r_1, of the reliability component defines the width of the distribution (in terms of σ_C) required to encompass a 95% cumulative probability. For normal distributions, a one-sided r_1-component could be defined as 1.65 σ_C as shown in Figure A.5. One-sided factors are applicable to parameters such as F_Q^N that are of concern only on one side of the calculational error distribution. Two-sided reliability factors would similarly be defined for normal distributions as 1.96 σ_C. This is also shown in Figure A.5.

The second component, r_2, is associated with the uncertainty in the determination of the standard deviation (1σ) itself. Due to statistical fluctuations, this relative uncertainty is obtained from statistical tables based on sampling theory for a 95% confidence level. Thus, the total reliability factor for a 95% probability at the 95% confidence level is given by

$$RF = \sigma_C r_1 r_2$$

FIGURE A.2

ONE & TWO SIDED RELIABILITY FACTORS

1) One-Sided Reliability Factor for Normal Distribution; $r_1 = 1.65$

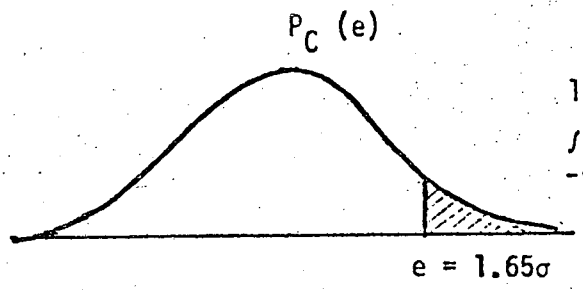

$$\int_{-\infty}^{1.65\sigma_C} P_C(e)de = 0.95$$

2) Two Sided Reliability Factor for Normal Distributions; $r_1 = 1.96$

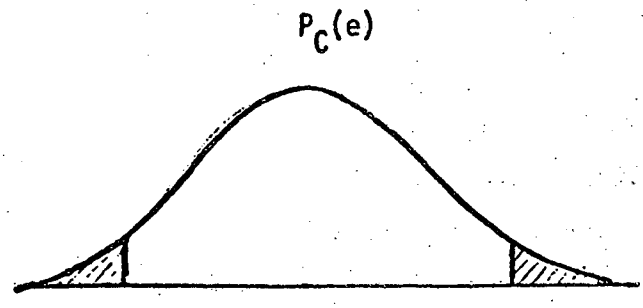

$$\int_{1.96}^{1.96} P_C(e)de = 0.95$$

NOTICE

THE ATTACHED DOCUMENT CONTAINS "PROPRIETARY INFORMATION" AND SHOULD BE HANDLED AS NRC "OFFICIAL USE ONLY" INFORMATION. IT SHOULD NOT BE DISCUSSED OR MADE AVAILABLE TO ANY PERSON NOT REQUIRING SUCH INFORMATION IN THE CONDUCT OF OFFICIAL BUSINESS AND SHOULD BE STORED, TRANSFERRED, AND DISPOSED OF BY EACH RECIPIENT IN A MANNER WHICH WILL ASSURE THAT ITS CONTENTS ARE NOT MADE AVAILABLE TO UNAUTHORIZED PERSONS.

COPY NO. 1

DOCKET NO. _____

CONTROL NO. _____

REPORT NO. _____

REC'D W/LTR DTD. _____

NRC Form 190
(4-78)

3.2 Temperature Coefficient Benchmarking

Measurements of the isothermal temperature coefficient at HZP are adequately made with a reactivity computer as there is usually no rod motion. When there is rod motion, there is usually sufficient time to allow the flux to stabilize.

The comparisons to the WPS ARMP model are summarized in Table 3.5 and Figure 3.2. It is apparent that a constant bias of -3.4 pcm/F exists with an RMS * scatter of 1.8 pcm/F.

*Root mean square = 1σ

REGULATORY DOCKET FILE COPY

The ITC reliability is defined as $\pm$ 5.7 pcm/F which represents a 95% probability ($\pm 1.65\sigma$) at the 95% confidence level that the measured ITC will be bounded by the predictions when the bias is included.

TABLE 3.5

MEASURED & CALCULATED ISOTHERMAL TEMPERATURE COEFFICIENTS

BOC, HZP, Kewaunee Cycles 1-4

Cycle	Rod Position Bank	Rod Position Steps	T_{MOD} (F)	Boron (ppm)	ITC $(\frac{pcm}{F})$ Meas.	ITC $(\frac{pcm}{F})$ Calc.	Diff pcm/F
1	D	190	538	1583	-2.4	- 4.9	-2.5
	C	196	540	1450	-3.6	-7.8	-4.2
	B	189	542	1317	-7.5	-12.4	-4.9
	A	201	545	1227	-11.3	-18.5	-7.2
	SB	194	544	1011	-14.1	-17.7	-3.0
2	D	204	540	1346	-4.0	-6.2	-2.2
3	D	162	540	1496	-4.4	-6.6	-2.2
4	D	200	543	1488	-3.9	-4.9	-1.0

Average difference = -3.4 $(\frac{pcm}{F})$

St'd deviation about avg. = 1.8 $(\frac{pcm}{F})$

FIGURE 3.2

MEASURED TO CALCULATED ISOTHERMAL TEMPERATURE COEFFICIENT DIFFERENCE VERSUS BORON

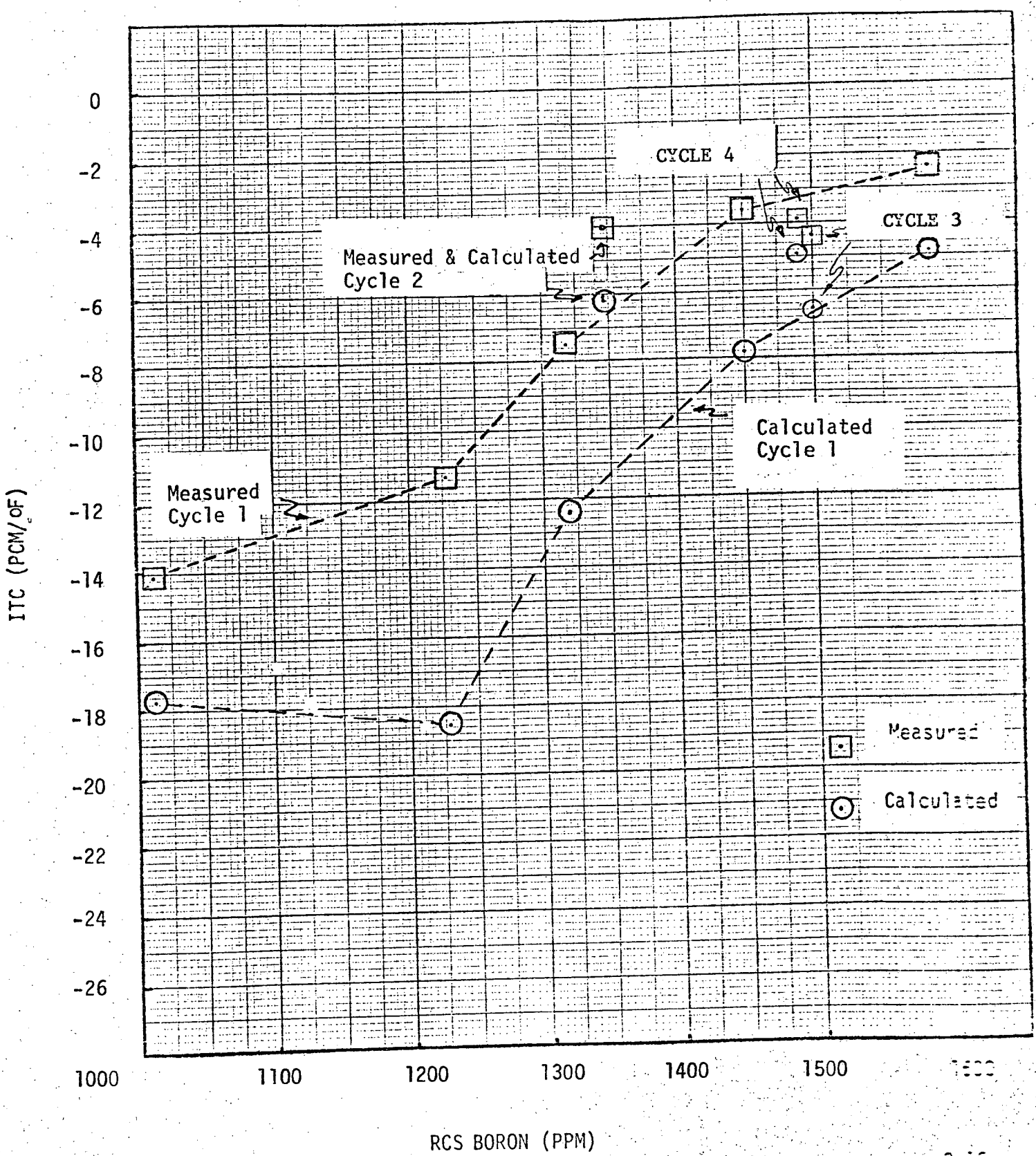

simulated with the WPS ARMP model. In addition to the measured signals from the moveable in-core fission detectors, core exit thermocouple data are also available from the ejected and dropped rod tests, and comparisons to model predictions of both in-core detectors and thermocouples are presented in Section 3.6.

[The prediction of the instrument signals is a two-step process. First, the average power within each node is calculated. Then, the instrument signal is predicted from the nodal power via instrument factors calculated from quarter-core PDQ's. The factors relate the fission rate in the instrument thimble to the average nodal power as a function of fuel design, nodal exposure, and control rod presence. The calculation of the instrument factors is very similar to the calculation of the radial peak to average pin factors and in fact is derived from the same set of PDQ's. It should be noted that all WPS PDQ calculations referenced in this report are of a two-dimensional geometry (XY planar).]

The calculation of peaking factors for Kewaunee safety evaluations is performed in a multi-step process beginning with the nodal code. For any core condition, the three-dimensional power distribution is calculated with 12-node axial resolution. The nodal values are then split axially with a single set of constant factors which account for the average axial flux gradients within a node and local flux perturbations caused by the assembly grid straps. The derivation of these factors is explained below.

[Both the average and the peak axial point power density values are obtained for each half-node in the core (121 assemblies x 24 half-nodes = 2904 half-nodes per flux map). The peak local pin power within each half-node is then obtained by applying radial PDQ ratios of peak to average fuel pin to the peak axial half-node power values above. The PDQ ratios are variable in fuel design, local burnup, and control rod presence.]

NAI PROPRIETARY

In order to derive uncertainty factors consistent with the above methodology, direct comparisons were made of the predicted and measured reaction rates in each half-node region for all flux maps tabulated in Table 3.8.

Each of the 19 flux maps consists of 61 measured axial data points in each of the 36 instrumented locations. These 61 values were grouped into approximately 3 points per ½-node. The total data base is therefore in excess of 40,000 measured data points. The constant axial factors discussed above were derived in a multi-step process. First, the model's upper and lower albedos were adjusted to provide a good overall agreement to the measured values of axial offset and core average axial peaking factors over three fuel cycles of operation. Using these albedos, reaction rates were then calculated and compared to each of the full power, steady-state flux maps described in Table 3.8. In all, this included some 28,500 measured and 11,200 calculated detector reaction rates (one calculated value per half-node). Two sets of 24 factors were derived from these comparisons. The first set, D1, is used to split the nodal calculations axially into half-nodes and was derived as the average ratio of the calculated reaction rate in the ½-node at level L (L=1 to 24) to the average measured reaction rate in the ½-node. The second set, D2, is used to calculate the peak reaction rate within the half-node and was derived as the average ratio of the peak measured reaction rate to the average measured reaction rate within the ½-node at level L (L=1 to 24). The factors are tabulated by axial level in Table 3.9. The effect of the grid strap positions can be clearly seen in both the D1 and D2 factors.

The standard deviation (average deviation, M, fixed as zero. See Appendix A.2) of the differences between the predicted peak axial reaction rate and the actual peak axial reaction rate (one of the three points) in each half-node has been calculated for each of the three cycles.

NAI PROPRIETARY

These results represent the combined effects of model accuracy and measurement uncertainty. It remains to conservatively estimate the model accuracy component using the statistical methods described in Appendix A.

In Figure 3.6, differences between measured and calculated incore detector signals are plotted as histograms.

In Figure 3.6A, measured and calculated channel integrated in-core detector signals are compared for steady state reactor conditions over the first three cycles of Kewaunee operation. In Figures 3.6B and C, maximum point values in each instrumented ½-node are compared for the same reactor state points.

In order to evaluate the measurement error distribution we need a reference for comparison. Comparisons of symmetric fuel assemblies in close proximity to each other are used here to perform this evaluation.

Differences in measured reaction rates in symmetric fuel assemblies can be due to either measurement error or real differences in local power levels. Significant differences in real powers might be expected in symmetric fuel locations that are separated by a large fraction of the core diameter if the core tilt is appreciable. This problem can be minimized if the comparison assemblies are chosen in close proximity to each other and the maps evaluated demonstrate negligible tilt.

In the Kewaunee reactor, the radial geometry of the instrument thimbles

NAI PROPRIETARY

introduces an additional symmetry constraint. They are not centered within the fuel assembly, thus creating a half-core symmetry rather than the octant symmetry of the fuel loading itself. This symmetry is shown in Figure 3.7, along with the eight symmetric fuel assemblies chosen for the evaluation of the measurement error distribution.

The average measured reaction rate in each ½-node region of the four northern members of the symmetric pairs shown in Figure 3.7 was subtracted from that of the southern members. The relative differences were grouped by axial position and plotted as measurement error histograms in Figure 3.8. Note that the upper and lower regions of the core have significantly broader distributions than those of the central regions. This is due primarily to small errors in the axial alignment of the in-core detector resulting in small axial displacements of the data for one member of the symmetric set relative to the other member. The differences in the symmetric measured signals due to these displacements are greatest in the upper and lower portions of the core where there is an overall steep flux gradient.

The value of ε (see Appendix A.2) appropriate to the data used in determination of the nodal power distribution uncertainties may now be evaluated. According to equation A.6, the maximum value ε is obtained by assuming the worst combinations of the observed means in Figures 3.6 and 3.8

The most conservative combination of the means, M_{MC}, for the evaluation of nodal uncertainties from the data in Figures 3.6 and 3.8 is as follows.

$$M_{MC} = +0.6\%$$

$$M_M = -0.3\%$$

NAI PROPRIETARY

These yield a value for ε as:

$$\varepsilon = 0.036$$

The nodal power distribution uncertainties for each cycle have been computed with the standard deviation of the differences between the measured and predicted instrument signals, the measurement uncertainties and equation A-5. The overall model uncertainty, σNODE, has been defined as a conservative upper bound to the individual cycle undertainties.

The data shown in Figure 3.6A demonstrate that the combined effects of measurement uncertainty and calculational uncertainty yield a difference distribution with a standard deviation of 2.5% for channel integrated signals. The net measurement uncertainty (1σ) for the channel integrated signals is conservatively estimated from the data shown in Figure 3.8 as 1.0% with a first moment of +0.1%. These estimates are based on the fact that the statistics for integrated values are better (smaller σ) than the statistics of the associated point components. This is demonstrated by Figures 3.6A and C. The value of ε appropriate to these results is computed using equation A.6 , the above moment, (M_M) and the moment of the measured to calculated difference distribution (M_{MC}) as shown in Figure 3.6A.

$$\varepsilon = .003$$

The assembly average power distribution uncertainties have been calculated using equation A-5. In a manner similar to that used for σNODE, the overall model uncertainty, σASSY, appropriate to the assembly average power distributions has been defined as a conservative upper bound to the individual cycle results.

$$\sigma ASSY = 0.027$$

NAI PROPRIETARY

A few of the individual comparisons of the measured and predicted reaction rates used to derive the uncertainties in Table 3.9 are shown in Figures 3.9 to 3.56. For each map, the differences in the channel and integrated values are shown along with the actual axial plots for an inner and outer instrument location. It should be noted that the axial plots have not been renormalized to make the integrals equal. The particular locations were chosen such that data would be available for each map. The inner thimble (#1) is the calibration thimble which is always measured and the outer thimble is either J3 (#24) or K4 (#31) which are nearly geometrically symmetric.

TABLE 3.8

MEASURED IN-CORE DETECTOR REACTION RATE DISTRIBUTIONS

KEWAUNEE

Fuel Cycle	Flux Map No	Cycle Exposure (GWD/MTU)	Power Level (%)	Rod Position (Steps)	Comments
1	1	0	~5	D=205	BOL, HZP
	12	0.2	37	D=152	K7 Ejected
	15	0.2	50	D=196	K7 Dropped
	34	1.8	92	D=198	
	66	6.6	97	D=218	
	108	12.6	98	D=217	
	131	16.2	98	D=217	EOC
2	133	0	~5	D=223	BOC, HZP
	154	1.4	100	D=219	
	163	3.5	96	D=223	
	179	6.1	97	D=225	
	194	8.5	98	D=228	EOC
3	195	0	~5	D=220	BOC, HZP
	207	1.4	98	D=228	
	215	3.4	99	D=228	
	221	5.9	100	D=228	
	235	10.0	100	D=228	
	244	12.8	99	D=228	EOC

TABLE 3.9

NODAL UNCERTAINTIES FOR KEWAUNEE

	NODE	½-NODE	σ_{NODE}	AXIAL FACTORS D1		D2
(core top)	12	24	.077	.857		1.171
		23	.067	1.238		1.053
	11	22	.034	.985	*	1.073
		21	.045	1.126		1.029
	10	20	.030	1.045		1.011
		19	.029	1.051		1.012
	9	18	.030	.949	*	1.050
		17	.036	1.028		1.010
	8	16	.030	1.021		1.005
		15	.029	1.021		1.004
	7	14	.031	.948	*	1.055
		13	.035	1.000		1.018
	6	12	.037	1.012		1.004
		11	.036	1.018		1.002
	5	10	.037	.983	*	1.021
		9	.037	.954	*	1.054
	4	8	.038	1.007		1.006
		7	.037	1.015		1.006
	3	6	.046	1.013		1.011
		5	.043	.936	*	1.051
	2	4	.049	1.041		1.016
		3	.042	.962		1.042
(core bottom)	1	2	.053	1.099		1.147
		1	.077	.666	*	1.166

*Approximate grid strap locations

The standard deviation about this bias is then 1.9%. Application of the statistics described in Appendix A requires a knowledge of the experimental or measurement error distribution. The ARMP documentation states only that the measured and calculated fission rate distributions were normalized such that the average value in the measured pins in the assembly is unity and that the standard deviation of the measurement error is 1.4%. This tends to make the first moment of the relative measurement error distribution zero. From the above results, values of ε on the order of a few percent were obtained from the data. For conservatism,aa value of 3% will be used here.

The CPM calculational uncertainty can now be computed using equation A.5 as shown below.

$$\sigma_C^2(\text{CPM}) = \sigma_{MC}^2(1 + \varepsilon) - \sigma_M^2$$

$$= (.019)^2(1.03) - (.014)^2$$

$$\sigma(\text{CPM}) = 1.3\% \qquad \text{bias (CPM - MEAS)} = -0.7\%$$

The one-sided, 95/95, confidence limit of σ(CPM) for a sample size of 15 is 1.3 + 0.6%.

NAI PROPRIETARY

A benchmark comparison of PDQ to CPM is described in Part I, Chapter 4 of the ARMP documentation. These results are reproduced in Figure 3.79 and tabulated in Table 3.13. The average (PDQ - CPM) peak pin bias for fuel pins adjacent to the water holes is +0.5% with a 1σ scatter about this bias of + 0.5%. These calculations represent a 14 x 14 fuel assembly at zero power and no burnup. In order to better define the PDQ - CPM differences for application to Kewaunee, new calculations were performed which compared the WPS ARMP models with CPM.

The WPS PDQ - CPM comparison calculations were made for a typical fuel type of 3.03 w/o over a burnup range of 0 to 18.0 GWD/MTU. The individual PDQ and CPM pin power distributions for the BOC and EOC cases are shown in Figures 3.80, 81 and 82. The differences between the PDQ and CPM pin powers for all fuel pins of higher than average power density are tabulated in Table 3.14. Since the average pin power has been normalized to unity, the values shown are typical of the peak pin to box ratios that might be applied to the peak nodal values of section 3.5 to compute the local F_Q^N values. (In actual practice, the values would be computed from quarter core rather than assembly geometry.)

The WPS calculations are consistent with the PDQ - CPM comparisons described in the ARMP documentation. Both demonstrate that PDQ overpredicts the peak pins relative to CPM. The WPS results demonstrate the fact that PDQ, with MND (mixed number densities), over-predicts the power in the fuel pins relative to CPM near the water holes. The lower bound of the peak pin to box (assembly average) power ratio as calculated by PDQ for Kewaunee is about 1.10. The average difference between

PDQ and CPM for peak pin to box ratios of 1.10 is 2.1%. This is obtained from a linear fit of the BOC and EOC pin-to-box differences in Table 3.14 versus the pin-to-box ratio. The standard deviation of the data about the line of best fit is 0.4%.

The uncertainties of CPM have now been defined with respect to experiment and the uncertainty of PDQ with respect to CPM. For conservatism, the uncertainty of PDQ with respect to experiment is defined as the statistical sum of the upper one-sided 95% confidence limits of σ(CPM-Meas) and σ(PDQ-CPM). These limits are as follows.

σ(CPM-Meas) < .019% (95% confidence, sample size N_1=15)

σ(PDQ-CPM) < .006% (95% confidence, sample size N_2=20)

$$\sigma(\text{PDQ-Meas}) < \sqrt{(.019)^2 + (.006)^2} = 2.0\%$$

The PDQ-Measurement bias is simply the sum of the CPM-Measurement bias and the PDQ-CPM bias (the bias is the negative of the average difference).

$$\begin{aligned}\text{Bias (PDQ-Meas)} &= \bar{x}(\text{CPM-Meas}) + \bar{x}(\text{PDQ-CPM}) \\ &= +0.7\% - 2.1\% \\ &= -1.4\%\end{aligned}$$

The lower, one-sided 95% confidence limit for difference between these two means is obtained from small sampling theory as -0.8% (sample sizes N_1=15, N_2=20)

Bias (PDQ-Meas) < -1.4% + 0.6% = -0.8%

However, for added conservatism, the PDQ bias will be defined as only half this magnitude, or only -0.4%.

In summary then, the statistics associated with PDQ calculations of peak pin-to-assembly average power ratios are as follows:

σ(PDQ-Meas) $\leq$ 2.0%

bias(PDQ-Meas) = -0.4%

TABLE 3.10

KRITZ EXPERIMENTS FOR

PWR LATTICES

PWR lattice 470F, <100 ppm

15x15 MO_2 **assembly with water holes and absorber rods surrounded by a uniform** UO_2 **lattice** (Fig 3.75)

Pu content in the MO_2 **rods**	**1.5 %**
UO_2 **rod enrichment**	**1.9 %.**

PWR lattice 470F, 1000 ppm

14x14 MO_2 **assembly with graded enrichment and with water holes, surrounded by** UO_2 **assemblies** (Fig 3.76)

Pu content in the MO_2 **rods**	**2 and 3 %**
UO_2 **rod enrichment**	**3 %.**

3.7.2 F_Q^N Reliability Factors

As explained in Section 3.5, the local pin peaks, F_Q^N, are calculated by multiplying peak nodal values by the PDQ pin-to-box ratios. These components are nearly independent in that the PDQ pin-to-box ratios are insensitive to changes in assembly power level, xenon inventory and boron concentration. Statistically as described below:

$$\sigma_{FQ}^2 = \sigma_{NODE}^2 + \sigma_{PDQ}^2$$

σ_{NODE} = Upper bound to the nodal uncertainties defined in Table 3.15

σ_{PDQ} = Upper, one-sided 95% confidence limit derived in section 3.7.1

σ_{FQ} = Upper, one-sided 95% confidence limit for the FQ uncertainty

The 95/95% confidence level reliability factors for F_Q are computed from the σ_{FQ} values above and the lower, one-sided 95% confidence limit for the PDQ bias defined in section 3.7.1. The results are shown by axial level in Table 3.15.

TABLE 3.15

F_Q^N RELIABILITY FACTORS FOR KEWAUNEE

	NODE	1/2 NODE	σNODE	F_Q RELIABILITY FACTORS (95/95% CONFIDENCE LEVEL)
(core top)	12	24	.100	.165
		23	.085	.140
	11	22	.070	.116
		21	.070	.116
	10	20	.050	.085
		19	.050	.085
	9	18	.045	.077
		17	.045	.077
	8	16	.045	.077
		15	.045	.077
	7	14	.045	.077
		13	.045	.077
	6	12	.045	.077
		11	.045	.077
	5	10	.045	.077
		9	.045	.077
	4	8	.045	.077
		7	.045	.077
	3	6	.065	.108
		5	.065	.108
	2	4	.065	.108
		3	.065	.108
(core bottom)	1	2	.085	.140
		1	.090	.148

3.7.3 $F_{\Delta H}$ Reliability Factor

The peak pin $F_{\Delta H}$'s are calculated as products of the nodal assembly average power values and the PDQ peak pin-to-box ratio.

In Section 3.5 the uncertainty (σ_{ASSY}) appropriate to the nodal assembly average power calculations was determined to be 2.7%. This is combined with the PDQ pin-to-box uncertainty (σ_{PDQ}) of 2.0% from section 3.7.1. to obtain σ_{FH}, the upper, one-sided 95% confidence limit for the $F_{\Delta H}$ in a manner similar to that of Section 3.7.2.

The 95/95% confidence level reliability factor appropriate to $F_{\Delta H}$ is then computed from the value of σ_{FH} above and the lower, one-sided 95% confidence limit for the PDQ bias defined in section 3.7.1.

$\sigma_{FH} = 0.051$

3.8 Delayed Neutron Parameters

The importance of the reliability of the calculated values of the delayed neutron parameters is primarily associated with the core β_{eff}. The uncertainties in the calculation of β_{eff} are composed of several components, the most important of which are listed below:

a. Experimental values of β, and λ, by nuclide;

b. Calculation of the spatial nuclide inventory. These uncertainties are addressed in Section 3.4;

c. Calculation of core average β as a flux weighted average over the spatial nuclide inventory;

d. Calculation of β_{eff} from the core average as $\beta_{eff} = \overline{I}*\beta$, where $\overline{I}$ = importance factor.

The experimental determinations of the β 's and λ 's are assumed to be accurate to within 1%. The most important nuclide concentrations with respect to core β are U^{238}, U^{235} and Pu^{239}. Table 3.7 of Section 3.4 demonstrate that the uncertainty in the calculation of these parameters is about 0.3% or less. Therefore, components a) and b) above are combined as 1.3%.

The uncertainty in the calculation of a core average β depends on the relative flux weighting of the individual assemblies in the core. For demonstration purposes, consider a three region core, each with a different average burnup and average β. This is typical of advanced PWR cycles in that about a third of the core has seen two previous cycles, a third only one previous cycle and a third is the feed fuel. Typical regional β's are given below:

A.1 Separation of Measurement and Calculational Uncertainties

Comparisons of measured and calculated reactor parameters include the effects of both the measurement and calculational uncertainties. Methods used in this report to isolate the calculational uncertainties are described below in terms of the following definitions:

X_T = true reactor parameter

X_M = measured reactor parameter

X_C = calculated reactor parameter

$e_M = X_M - X_T$ = measurement error

$e_C = X_C - X_T$ = calculation error

$e_{MC} = X_M - X_C$ = observed differences

$\mu_i = \bar{e}_i$ = mean error

$\sigma_i = \sqrt{\frac{1}{N}\Sigma(e_i - \mu_i)^2}$ = standard deviation

$m_i^2(A) = \frac{1}{N}\Sigma(e_i - A)^2$ = second moment about an arbitrary origin A

If e_M and e_C are independent, then the following relationships exist.[7,8]

(A - 1) $\sigma_C^2 = \sigma_{MC}^2 - \sigma_M^2$

(A - 2) $\mu_c = \mu_M - \mu_{MC}$

Once the σ_C and μ_C have been calculated from historical data, they could be used to apply conservatism to future calculations of reactor parameters, X_C, as follows:

(A - 3) $X_C' = X_C - \mu_C \pm r_1 r_2 \sigma_C$

The factors r_1 and r_2 are defined as described in Section A.2 to provide a 95% probability at the 95% confidence level that X_C' is conservative with respect to the true value, X_T.

It is apparent that the mean, μ_C, plays a key role in the above procedure. In most cases, μ_C is found to vary somewhat from experiment to experiment. It is convenient, therefore, to define a procedure which is independent of small variations in μ_C. To accomplish this, the following procedure has been used in this report. Estimates of the means, μ_i, have been made using the empirical data contained in this report and then the variances estimated as the second moment about these means. The estimates of the means may be obtained as direct calculation of the mean in which case the second moment is identically the variance. This is the case for Section 3.2, Temperature Coefficient Benchmarking. In Section 3.7.1 however, the mean was chosen as a representative value. In either case, these means will remain fixed for future applications of equation (A - 3) and the estimates of the variances will be obtained using the second moment about these fixed means.

If the fixed mean, μ_i', is also the true mean, μ_i, then the procedure yields exactly the variance. If the true mean differs from the fixed mean, the procedure yields an over estimate of the variance, σ_i^2, since the statistics are related as follows[8]:

$$(A - 4)\quad m_i^2 = \sigma_i^2 + (\mu_i - \mu_i')^2$$

A small complication must now be addressed. Although the above procedure results in conservative (if not exact) estimates of the components σ_{MC}^2 and σ_M^2, the difference in the two could be slightly non-conservative. The following modification to equation (A - 1) is therefore implemented to compensate.

For a given distribution, i, the following relationship exists[8]:

$$m_i^2(A) = \sigma_i^2 + \Delta\mu_i^2$$

NAI PROPRIETARY

μ_i = observed mean

σ_i = standard deviation

$m_i^2(A_i)$ = second moment about an arbitrary origin A_i

$\Delta\mu_i = \mu_i - A_i$

Substituting this into equation (A - 1) and rearranging terms results as follows:

$$(A - 5) m_C^2 = M_{MC}^2 (1 + \varepsilon) - m_M^2$$

$$(A - 6) \quad \varepsilon = \frac{+2\Delta\mu_M}{m_{MC}^2} (\Delta\mu_M - \Delta\mu_{MC})$$

Equation (A - 5) is used to provide a conservative estimate of m_C^2 in terms of the errors in the choice of the means; μ_M and μ_{MC}; and the second moment m_{MC}^2. Note that for applications of ε in equation (A - 5), ε must be positive or zero. ε is positive when $\Delta\mu_M^2 > \Delta\mu_M \Delta\mu_{MC}$. A numerical example of a typical application may be instructive. In comparing the measured and calculated in-core detector reaction rates in Section 3.5, the following statistics were generated:

$M_{MC}^2(A = 0) = (.039)^2$	Figure 3.6B
$\mu_{MC} = M_{MC} = +0.006$	Figure 3.6B
$\mu_M = M_M = -0.003$	Figure 3.8, nodes 3 & 4
$m_M^2 (A = 0) = (.012)^2$	Figure 3.8, nodes 3 & 4

NAI PROPRIETARY

Since the moments were computed about an origin of zero, the $\Delta\mu_i$ can be estimated as the μ_i.

$$\varepsilon = \frac{+2\Delta\mu_M}{m_{MC}^2}(\Delta\mu_M - \Delta\mu_{MC})$$

$$= \frac{+2(-.003)(-.003 - .006)}{(.039)^2}$$

$$= +0.036$$

$$m_C^2 = m_{MC}^2\ (1 + \varepsilon) - m_C^2$$

$$= (.039)^2(1.036) - (.012)^2$$

$$m_C^2 = (.038)^2$$

$$\sigma_C^2 \leq \sqrt{m_C^2} = .038$$

It is apparent that there is minimal impact to the resultant calculational uncertainty if the means, μ_M and μ_{MC}, are fixed as representative values and the standard deviations are estimated as the second moment about the fixed means.

All parameters labeled as σ in the context of this report have been estimated using the above procedure. In Section 3.5, the origin for the moments were all taken as zero.

NAI PROPRIETARY

A.2 Reliability Factors

It is the objective of this section to define reliability factors which are to be used to increase/decrease calculated results to the point where there is a 95% probability at the 95% confidence level that they are conservative with respect to actual reactor performance. Thus there are two components to be considered, termed r_1 and r_2.

A distribution of differences between truth and calculation for a given parameter is characterized by its standard deviation, σ_C. The first component, r_1, of the reliability component defines the width of the distribution (in terms of σ_C) required to encompass a 95% cumulative probability. For normal distributions, a one-sided r_1-component could be defined as 1.65 σ_C as shown in Figure A.5. One-sided factors are applicable to parameters such as F_Q^N that are of concern only on one side of the calculational error distribution. Two-sided reliability factors would similarly be defined for normal distributions as 1.96 σ_C. This is also shown in Figure A.5.

The second component, r_2, is associated with the uncertainty in the determination of the standard deviation (1σ) itself. Due to statistical fluctuations, this relative uncertainty is obtained from statistical tables based on sampling theory for a 95% confidence level. Thus, the total reliability factor for a 95% probability at the 95% confidence level is given by

$$RF = \sigma_C r_1 r_2$$

FIGURE A.2

ONE & TWO SIDED RELIABILITY FACTORS

1) One-Sided Reliability Factor for Normal Distribution; $r_1 = 1.65$

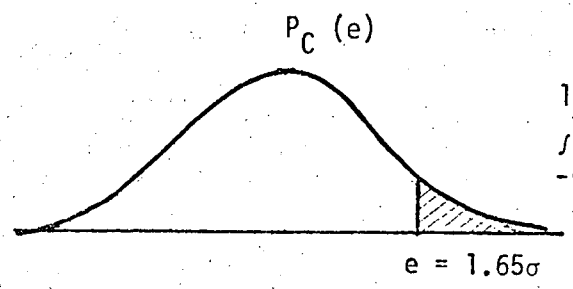

$$\int_{-\infty}^{1.65\sigma_C} P_C(e)de = 0.95$$

2) Two Sided Reliability Factor for Normal Distributions; $r_1 = 1.96$

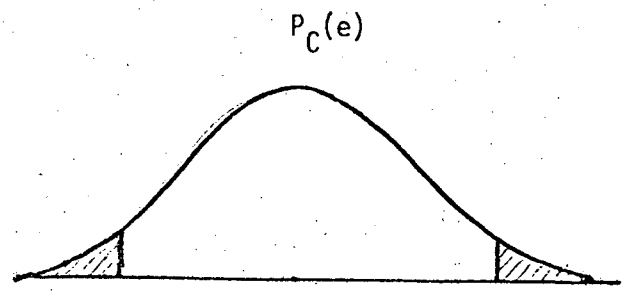

$$\int_{1.96}^{1.96} P_C(e)de = 0.95$$